Springer

Journal of
Mechanical
Science and
Technology

Journal of Mechanical Science and Technology 22 (2008) 819~826

www.springerlink.com/content/1738-494x

An analysis of flow and screech tone from supersonic axisymmetric jet at the initial stage

In Cheol Lee* and Duck Joo Lee

Department of Mechanical Engineering Division of Aerospace Engineering Korea Advanced Institute of Science and Technology 373-1 Guseong, Yuseong, Daejeon 305-701, Korea

(Manuscript Received November 5, 2007; Revised December 23, 2007; Accepted December 24, 2007)

Abstract

The screech tone from jet Mach number 1.18 is numerically calculated from the initial stage. A fourth-order optimized compact scheme and fourth-order Runge-Kutta method are used to solve the 2D axisymmetric Euler equation. Pulse jet problem with Mach number 1.56 is solved to validate the present method. Not only two important components of generating screech tones, shock cell structure and vortices, but also the transient behavior of the screech tone are investigated at the initial stage. Additional time is necessary to generate periodic screech tone after formation of shock cell structures. As time goes on, the location of the vortex generation becomes fixed near the nozzle exit, which is farther downstream initially, and the screech tone becomes periodic. The FFT results of three different periods are compared. It is observed that the component of lower frequency is dominant at the beginning, and the component of the screech tone becomes dominant as time increases. It can be concluded that the screech tones can be also numerically reproduced at the initial stage with the present inviscid method.

Keywords: Supersonic jet noise; Screech tone; Shock cell; Instability wave; Computational aeroacoustics (CAA)

1. Introduction

When supersonic jet flow is generated, jet noise is also generated from the jet flow. Supersonic jet noise has clear directivity patterns depending on the noise component. Supersonic jet noise consists of three principal components: turbulent mixing noise, broadband-shock-associated noise, and screech tones [1]. Turbulent mixing noise radiates downstream due to a large-scale turbulence structure as a supersonic Mach wave. Shock-associated noise and screech tone propagate upstream due to shock cell structure, which are only generated by an under-expanded jet. Shock-associated noise is produced by the interaction between a shock cell and a vortex, whereas screech tone is produced by a feedback loop near the nozzle exit.

For over fifty years, research on screech tone has been conducted via experimental and theoretical methods. Numerical simulations have been widely used recently because numerical computation has become so powerful. One of the common methods is turbulent modeling [2, 3]. The other method is direct numerical simulation (DNS) [4]. Large eddy simulation (LES) [5] is another method which can simulate jet noise numerically. However, the characteristics of screech tone and its transient behavior at the initial stage have not been investigated by either experiments or numerical simulations. So, additional investigations on when the screech tone begins to be generated and how the screech tone becomes periodic are necessary.

In this work, an underexpanded supersonic jet with Mach number 1.18 is numerically calculated from the initial stage to investigate the transient behavior of the screech tone after validation of present method. Formation of shock cell structures and generation of vortices are observed. The formation process of jet flow,

*Corresponding author. Tel.: +82 42 869 3756, Fax.: +82 42 869 3710
E-mail address: essence@kaist.ac.kr
DOI 10.1007/s12206-007-1210-7

such as shock cell structures and vortices, and the FFT results of three different periods at the initial stage are compared to understand the generation of the screech tone noise from the beginning of the jet flow. Additionally, the variation of the screech tone wavelengths with respect to jet Mach number is investigated and compared with other results.

2. Governing equations and numerical methods

In this work the Euler equation is used and no effect of viscous flow is considered. All the governing equations of motion for the axisymmetric inviscid flow are:

$$\frac{\partial \mathbf{Q}}{\partial t} + \frac{\partial \mathbf{E}}{\partial x} + \frac{\partial \mathbf{F}}{\partial y} + \mathbf{H} = 0 \tag{1}$$

where

$$\mathbf{Q} = \begin{bmatrix} \rho \\ \rho u \\ \rho v \\ \rho e_t \end{bmatrix}, \mathbf{E} = \begin{bmatrix} \rho u \\ \rho u^2 + p \\ \rho uv \\ (\rho e_t + p)u \end{bmatrix}, \quad \mathbf{F} = \begin{bmatrix} \rho v \\ \rho vu \\ \rho v^2 + p \\ (\rho e_t + p)v \end{bmatrix}, \mathbf{H} = \frac{1}{\mathrm{y}} \begin{bmatrix} \rho v \\ \rho vu \\ \rho v^2 \\ (\rho e_t + p)v \end{bmatrix} \tag{2}$$

To accurately simulate a screech tone, the flow near the nozzle exit should be simulated correctly and the wave, which propagates upstream with relatively small amplitude, should be analyzed precisely. Hence, to successfully analyze a screech tone, the CAA method (computational aeroacoustics), which has high-resolution and high-order is used. In this work, fourth-order OHOC (optimized high-order compact) [6, 7] schemes for the evaluation of spatial derivatives and the fourth-order Runge-Kutta scheme for integration in time are used. The adaptive nonlinear artificial dissipation model [8] is also used to remove unwanted numerical dissipation. Generalized characteristic boundary conditions [9] and absorbing layer, which is shown as gray thick line along the boundary in Fig. 1, are used as the time-dependent boundary conditions to prevent unwanted non-physical reflections around the computational boundaries. Fig. 1 shows the entire computation domain schematically. The domain consists of three sub-domains. The numerical domain extends 50 times the nozzle exit diameter in the x direction and 30 times the nozzle exit diameter in the y direction. The total number of grid points is about 100,000 including absorbing layer, and grid points are condensed around the nozzle exit both in the x and y directions.

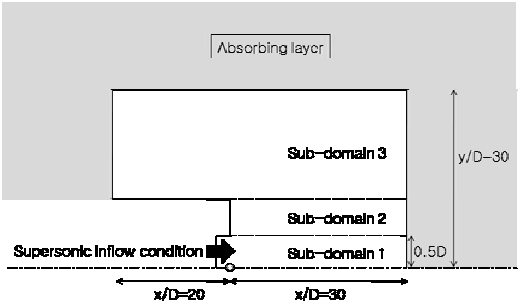

Fig. 1. Schematic view of computational domain and boundary conditions.

Initially, the whole computational domain is set to ambient flow conditions and the supersonic inflow condition at the nozzle exit is specified as follows [10] with the use of ideal gas isentropic relations:

$$p = \frac{1}{\gamma}\left[\frac{2+(\gamma-1)M^2}{\gamma+1}\right]^{\frac{\gamma}{\gamma-1}}$$
$$\rho = \frac{\gamma(\gamma+1)p}{2T_r} \tag{3}$$
$$u = \left(\frac{2T_r}{\gamma+1}\right)^{\frac{1}{2}}, \quad v = 0$$

In this research, T_r is equal to 1, because only cold jet condition is considered in this work.

3. Numerical results

3.1 Validation of present method

Using the numerical algorithm described earlier, we have numerically simulated the pulse jet problem. Through the analysis of pulse jet problem, the motion of first produced unsteady Mach disk and the position of the first generated vortex are investigated. A pulse jet is generated from a shock tube; the pressure ratio of the shock tube is 8.7 and its Mach number is 1.56. Fig. 2 shows two instantaneous density contours of

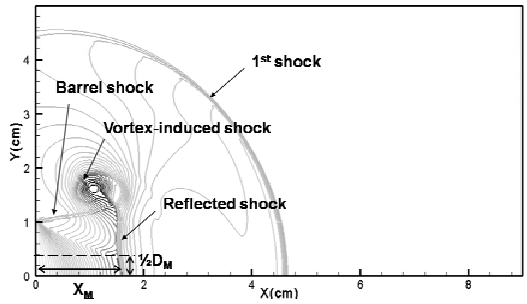

(a) t = 97 μs

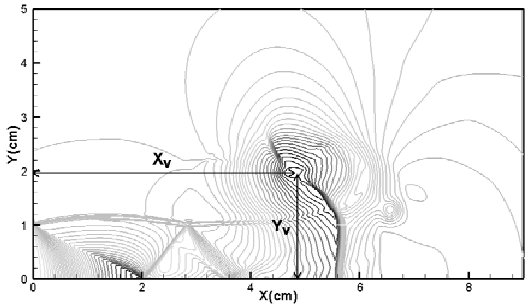

(b) t = 291 μs

Fig. 2. Instantaneous density contours of M=1.56 pulse jet at two different times.

the M=1.56 pulse jet and introduces main jet structures.

To see if the first unsteady Mach and the first vortex are numerically simulated properly, the diameter of the unsteady Mach disk (D_M), the axial distance of the unsteady Mach disk (X_M), the axial coordinate of the first vortex (X_V), and the radial distance of the first vortex (Y_V) described in Fig. 2 are calculated and compared with experimental and numerical results [11] and other numerical result [12]. Ishii et al. solved Euler equations and Kim solved the Navier-Stokes equation. Fig. 3 shows the diameter and the axial distance of the unsteady Mach disk, and Fig. 4 shows the position of the first generated vortex. Results of the Mach disk in Fig. 3 are shown only up to t=150$\times 10^{-6}$ sec since the unsteady Mach disk disappears to make the first shock cell. First shock cell and an expansion wave are generated after t=150$\times 10^{-6}$ as shown in Fig. 2. Present results show a good agreement with experimental data and other numerical results. It seems that the numerical algorithm described earlier can properly simulate the flow motions at the initial stage.

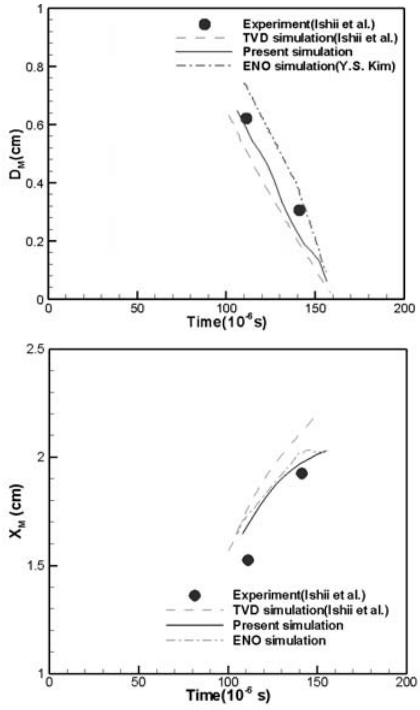

Fig. 3. Diameter and axial distance of unsteady Mach disk with respect to time generated from a pulse jet of pressure ratio 8.7 (M=1.56).

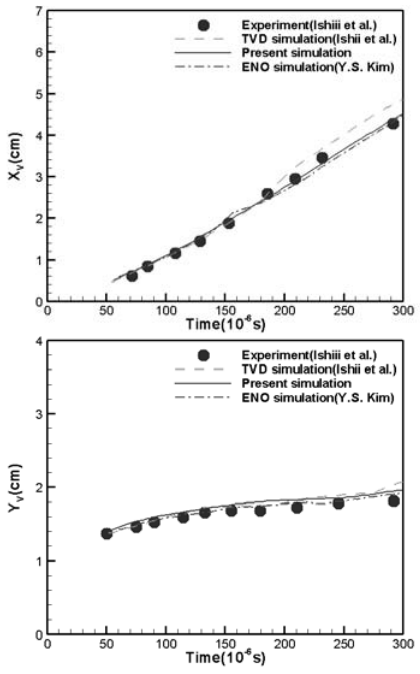

Fig. 4. Axial coordinate and radial distance of first vortex with respect to time generated from a pulse jet of pressure ratio 8.7 (M=1.56).

3.2 Formation of shock cell structures

Fig. 5 shows the instantaneous density contour of a Mach number 1.18 near the nozzle exit. It is observed that shock cells are formatted and vortices are being generated from the mixing layer of supersonic jet flow.

The formation of shock cell structures is observed from the initial stage. Fig. 6 shows the instantaneous pressure contour near the nozzle exit with respect to non-dimensional time. The first shock cell is formatted due to the barrel shock and the reflected shock, defined in Fig. 2(a) after the generation of vortex. They are also observed in Fig. 6(a). In Fig. 6(b), the second shock cell appears at about x/D=0.8 and the reflected shock propagates to the farther downstream. They seem to be overlapped since the propagation speed of the first generated vortex is different from the speed of shock cell formation. The speed differences between vortex propagation and shock cell formation are observed more clearly in Fig. 6(c) and (d). In Fig. 6(f), four shock cells are observed at t=11; however, the outline of the fourth shock cell is not so clear compared to outlines of first three shock cells. This is because the strength of the shock cell weakens as the number of shock cells increases.

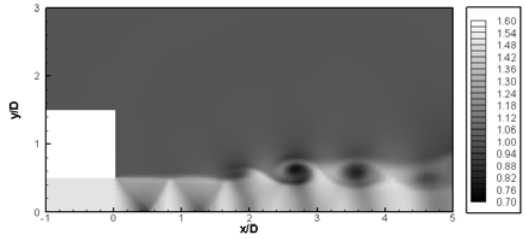

Fig. 5. Instantaneous density contour for jet Mach number 1.18.

Fig. 7 is a pressure signal measured at one point of the nozzle exit plane (x/D=0, y/D=0.889) shown as a star (☆) in Fig. 5 to investigate the noise charac-

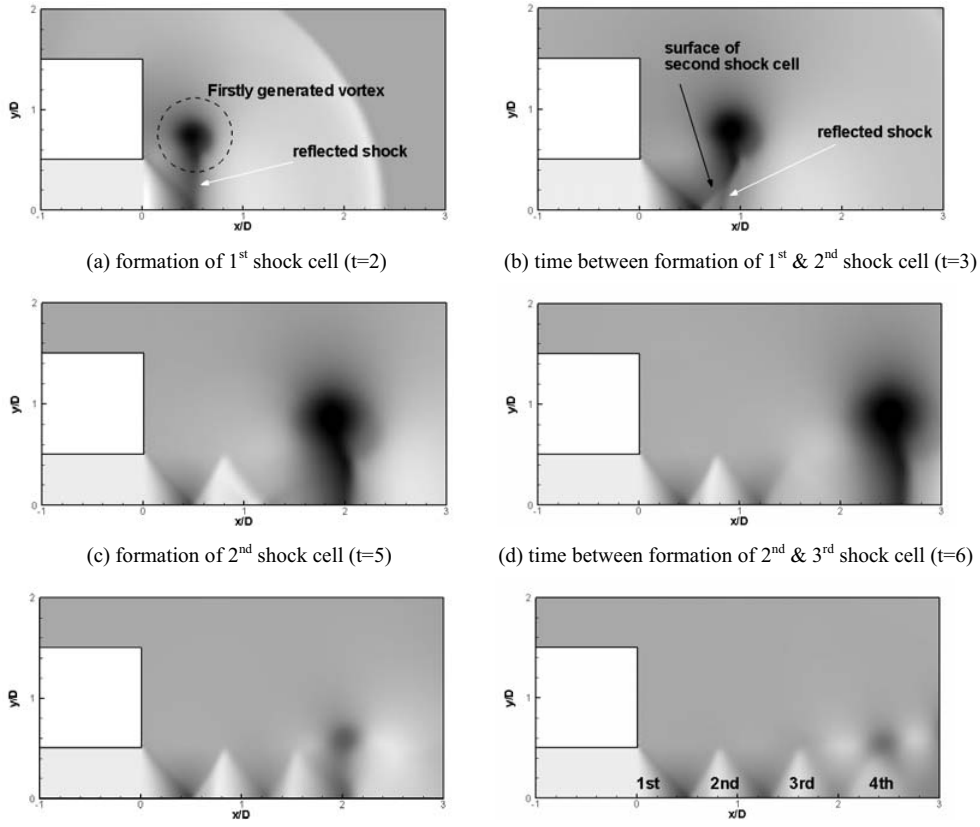

(a) formation of 1st shock cell (t=2)

(b) time between formation of 1st & 2nd shock cell (t=3)

(c) formation of 2nd shock cell (t=5)

(d) time between formation of 2nd & 3rd shock cell (t=6)

(e) formation of 3rd shock cell (t=8)

(f) formation of 4th shock cell (t=11)

Fig. 6. Observation of shock cell structure formation with respect to non-dimensional time (t = 2~11) by instantaneous pressure contour.

teristics of the screech tone at the initial stage. The shock cell structures, which are the main source of supersonic jet noise, are formatted at t=11 or marked as 't_{sc}' in Fig. 7. The pressure signal becomes periodic after t=60 and this periodic signal is the pressure signal of the screech tone. So it can be concluded that the screech tones are not generated just after the formation of shock cell structure and additional time is necessary after the formation of shock cell structures to generate periodic noise propagating upstream, or screech tone.

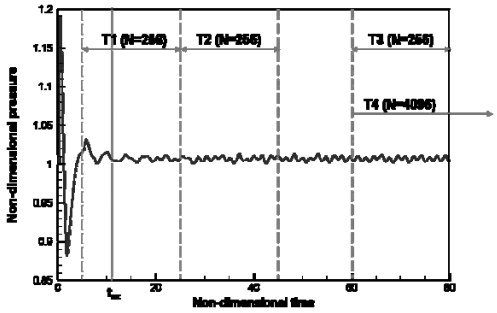

Fig. 7. Pressure signal measured at one point (x/D=0, y/D=0.889) of nozzle exit plane for jet Mach number 1.18.

3.3 Generation of vortices and instability waves

Another important component for generating screech tone is vortices since the screech tone is generated by the interaction of shock cells and vortices. Fig. 8 shows the instantaneous density contour at six different non-dimensional times at t=10, 20, 30, 40, 60, and 80. At t=10 in Fig. 8(a), the first generated vortex is observed and the second vortex is generated. To understand the transient motion of vortices, perturbations of the mixing layer from t=20 to t=80 are observed (dashed box in Figs. 8(b)-(f)). Up to t=40, the perturbation of the mixing layer begins around x/D=2 or so and a vortex is generated after x/D=2 as shown in Fig. 8(d). However, as time increases, it is observed that the perturbation of the mixing layer begins around x/D=1.5 and the vortex is generated before x/D=2, dashed circle in Figs. 8(e) and (f), which can be also observed at Fig. 5(a). It can be concluded that the distance between the location of vortex generation and the nozzle exit, which is in the farther downstream initially, becomes shorter as time increases. The distance is fixed at t=60 and the pressure signal becomes periodic.

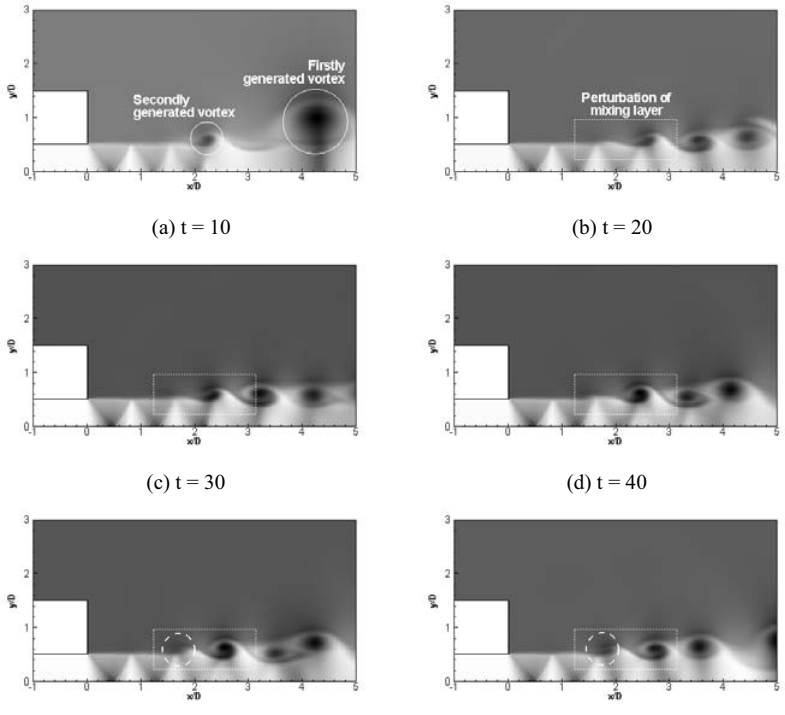

(a) t = 10 (b) t = 20

(c) t = 30 (d) t = 40

(e) t = 60 (f) t = 80

Fig. 8. Instantaneous vorticity contour with respect to non-dimensional time.

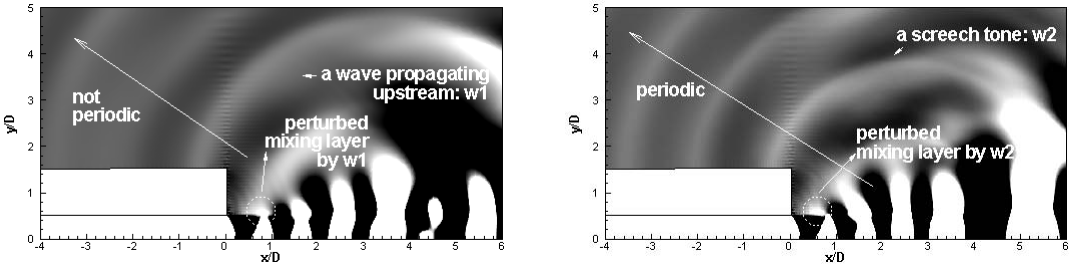

(a) t = 20 (b) t = 80

Fig. 9. Instantaneous pressure contours with adjusted contour level ($0.99<p/p_a<1.01$) for jet Mach number 1.18 at two different non-dimensional times.

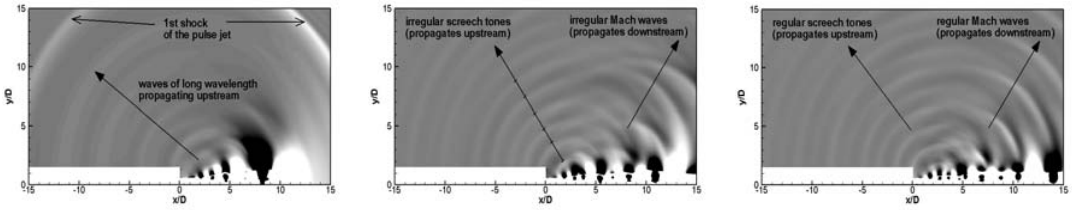

(a) t=20 (in period T1) (b) t=40 (in period T2) (c) t=80 (in period T3)

Fig. 10. Visualization of noise propagation ($0.99<\rho/\rho_a<1.01$) of Mach number 1.18 jet at three different non-dimensional times.

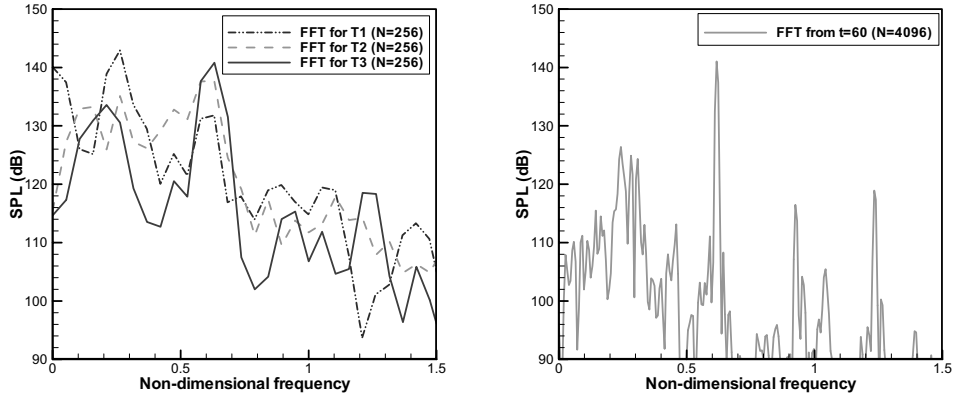

(a) FFT results of three different periods T1, T2 and T3 (N=256) (b) FFT result for longer period T4 (N=4096)

Fig. 11. FFT results for various time periods.

To observe the reduction of the distance, the instantaneous pressure contours at two different non-dimensional times at t=20 (generating transient tones) and at t=80 (generating periodic tones) are compared. An adjusted level ($0.99<p/p_a<1.01$) is applied in the figure to observe the jet noise, of which amplitude is only 1 percent or 0.1 percent of ambient pressure. Fig. 9(a) is the instantaneous pressure contour at t=20. Several waves propagate upstream, which are not periodic. Some part of each wave hits the nozzle exit plane and the mixing layer is perturbed due to the sound wave at the nozzle exit plane. This causes an increase of the instability of the mixing layer. It changes the location of vortex generation in Fig. 8. As time increases, the location of vortex generation is adjusted and fixed. If the location of vortex generation is fixed, the location of interaction between shock cells and vortices is also fixed, so the waves become periodic as shown in Fig. 9(b). This is the screech tone feedback process.

To investigate the generation and the transient behavior of the screech tones, three non-dimensional time periods, T1, T2, and T3, are chosen as shown in Fig. 7. The instantaneous density contours with adjusted contour level ($0.99<p/p_a<1.01$) at three different non-dimensional times, t=20 (in period T1), t=40 (in period T2), t=80 (in period T3), are shown in Fig. 10 to observe the noise propagation. Fig. 11(a) shows the results of Fast Fourier Transform (FFT) for three time periods for more quantitative investigation. At each period, 256 data are used for FFT. The sampling ration is 0.075 non-dimensional time so the non-dimensional sampling frequency is about 13.3. The non-dimensional Nyquist frequency is about 6.67 and the non-dimensional frequency resolution is about 0.052. The dashed-dot-dot line is the FFT result of early period (T1), the dashed line is the FFT result of middle period (T2), and the solid line is FFT result of later period (T3).

In the early period (T1), the first shock of the pulse jet is observed and the waves of long wavelength are observed in Fig. 10(a). The non-dimensional frequency of these waves is about 0.25 as shown in Fig. 11(a) (dashed-dot-dot line). In the middle period (T2), the waves propagating upstream and downstream, or the screech tones and the Mach waves are observed; however, they are neither periodic nor regular. The wavelengths of the screech tones are not regular as shown in Fig. 10(b). The spectral characteristic of the irregular screech tones is shown as a dashed line in Fig. 11(a). The amplitude of non-dimensional frequency equal to 0.25 becomes smaller and the amplitude of non-dimensional frequency equal to 0.60 becomes larger. And the component of non-dimensional frequency equal to 0.50 also becomes larger. In the later period (T3), the screech tones and the Mach waves become periodic as shown in Fig. 10(c). In Fig. 11(a), it is observed that the component of non-dimensional frequency equal to 0.50 becomes small and the higher frequency component of non-dimensional frequency equal to 0.60 is dominant. This means that the screech tone becomes regular in period T3, which was not regular in period T2 since the location of vortices generation is fixed after t=60 as shown in the earlier observation (Fig. 8).

To obtain more quantitative characteristics of dominant component after t=60, a longer period is selected for FFT. The longer period, which is shown as T4 in Fig. 7, begins at t=60, and 4096 data are acquired with the same sampling frequency of T1, T2 and T3 and the non-dimensional frequency resolution is about 3.26×10^{-3}. So the result of T3 has 16 times higher resolution than that of T1 or T2. Fig. 11(b) is the result of FFT for the longer period T4. The non-dimensional frequency of the dominant component, screech tone, is about 0.617 so its non-dimensional wavelength is about 1.62, since the non-dimensional wavelength can be obtained from equation (4). And the amplitude of screech tone is about 142 dB.

$$\frac{\lambda}{D}=\frac{a_\infty}{fD} \tag{4}$$

Since it is known that the axisymmetric screech tone is generated when the jet Mach number is smaller than 1.20 [13], two additional jet Mach numbers 1.12, 1.15 are selected and the non-dimensional wavelengths are obtained after performing the numerical simulations at those jet Mach numbers. The non-dimensional wavelengths are obtained from the FFT of 4096 data with same sampling ratio and frequency resolution of T4. Fig. 12 shows the non-dimensional wavelength variation of axisymmetric screech tone with respect to Mach number. The present result shows a good agreement with experimental results [13]. Another numerical result [2] shows an over-predicting trend (other mode) up to jet Mach number 1.18. It can be concluded that the present inviscid method simulates the axisymmetric screech tone properly and shows the generation of screech tone from the initial stage.

4. Conclusions

In the present research, we simulate an axisymmetric screech tone from M=1.18 jet flow from the initial stage with the help of a high-order, high-resolution computational aeroacoustics (CAA) scheme. To validate the developed program, traces of the unsteady Mach wave and the first vortex of jet Mach number 1.56 at the initial stage are compared, and the result shows a good agreement with other results. The transient behavior of the screech tone is investigated at the initial stage for the first time. Formation of two important components for generating screech tones (four shock cell structures and vortices generation) are also observed with respect to time. Shock cells are formatted at t=11. However, additional time is needed to generate the periodic screech tone. The location of vortex generation is fixed after t=60 and the pressure

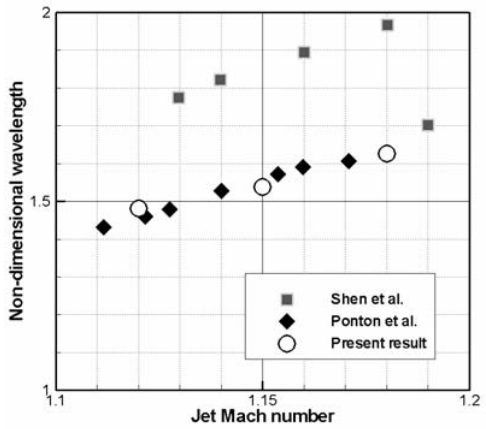

Fig. 12. Non-dimensional wavelength variation of the axisymmetric screech tone.

signal becomes periodic. FFT results in the early period (t=5-25), in the middle period (25-45) and in the later period (t=60-80) are compared. It is observed that the component of the screech tone is not dominant, but the component of lower frequency is dominant at the beginning, and the component of the screech tone becomes dominant as time increases. It can be concluded that the screech tones can be simulated clearly with the present inviscid method by observing the transient behavior of the supersonic jet flow and the screech tone.

Acknowledgment

This work was supported by the Space Technology Program of KISTEP (Korea Institute of Science and Technology Evaluation and Planning).

Nomenclature

M : Jet Mach number
D : Diameter of nozzle exit
a_∞ : Speed of sound propagation
x : X direction
y : Y direction
ρ : Density
u : Velocity in x direction
v : Velocity in y direction
p : Pressure
T_r : Reservoir temperature
e_t : Total internal energy
f : Frequency of screech tone
λ : Wavelength of screech tone
γ : Specific heat ratio

References

[1] C. K. W. Tam, Supersonic jet noise, *Annual Review of Fluid Mechanics* 27 (1995) 17-43.
[2] H. Shen and C. K. W. Tam, Numerical simulation of the generation of axisymmetric mode jet screech tones, *AIAA Journal* 36 (10) (1998) 1801-1807.
[3] Y. S. Kim and D. J. Lee, Acoustic properties associated with nozzle lip thickness in screeching jets, *Journal of Mechanical Science and Technology* 21 (5) (2007) 764-771.
[4] J. B. Freund, Acoustic sources in a turbulent jet: a direct numerical simulation study, AIAA/CEAS Aeroacoustics Conference and Exhibit, Bellevue, WA, (1999) 1-13.
[5] C. Bogey, C. Bailly and D. Juve, Computation of the sound radiated by a 3-D jet using large eddy simulation, AIAA/CEAS, Aeroacoustics Conference and Exhibit, Lahaina, HI, (2000) 2000-2009.
[6] J. W. Kim and D. J. Lee, Optimized compact finite difference schemes with maximum resolution, *AIAA Journal* 23 (5) (1995) 887-893.
[7] J. W. Kim and D. J. Lee, Implementation of boundary conditions for optimized high-order compact scheme, *Journal of Computational Acoustics* 5 (2) (1997) 177-191.
[8] J. W. Kim and D. J. Lee, Adaptive nonlinear artificial dissipation model for computational Aeroacoustics, *AIAA Journal* 39 (5) (2001) 810-818.
[9] J. W. Kim and D. J. Lee, Generalized characteristic boundary conditions for computational Aeroacoustics, *AIAA Journal* 38 (11) (2000) 2040-2049.
[10] P. Jorgenson and C. Loh, Computing axisymmetric jet screech tones using unstructured grids, 38th AIAA/ASME/SAE/ASEE Joint Propulsion Conference and Exhibit, Indianapolis, Indiana, (2002) AIAA-2002-3889.
[11] R. Ishii, H. Fujimoto, N. Hatta and Y. Umeda, Experimental and Numerical Analysis of Circular Pulse Jets, *Journal of Fluid Mechanics* 392 (1999) 129-153.
[12] Y. S. Kim, Analysis of radiated noise from internal duct flow and external jet using high-resolution schemes, Ph.D. thesis, KAIST (2001).
[13] M. K. Ponton and J. M. Seiner, The effects of nozzle exit lip thickness on plume resonance, *Journal of Sound and Vibration* 154 (3) (1992) 531-549.